Supplementary Material for The Effect of Intrinsic Quantum Fluctuations on the Phase Diagram of Anisotropic Dipolar Magnets

Tomer Dollberg,[1] Juan Carlos Andresen,[1] and Moshe Schechter[1]
[1] *Department of Physics, Ben-Gurion University of the Negev, Beer Sheva 84105, Israel*

EFFECTIVE HAMILTONIAN WITH OFFDIAGONAL DIPOLAR (ODD) TERMS INCLUDED

Pure $LiHoF_4$ forms a tetragonal structure with lattice constants $a = 5.175$ Å and $c = 10.75$ Å, as shown in Fig. 2a of the main text. There are four Ho^{3+} ions per unit cell which form a lattice with a basis with coordinates $(0, 0, \frac{1}{2})$, $(0, \frac{1}{2}, \frac{3}{4})$, $(\frac{1}{2}, \frac{1}{2}, 0)$ and $(\frac{1}{2}, 0, \frac{1}{4})$ [1]. The complete Hamiltonian of $LiHoF_4$ in a transverse magnetic field is given by [1, 2]

$$H = \sum_i V_C(\boldsymbol{J}_i) - g_L\mu_B \sum_i B_x J_i^x + \frac{1}{2}(g_L\mu_B)^2 \sum_{i\neq j} V_{ij}^{\mu\nu} J_i^\mu J_j^\nu + J_{\rm ex} \sum_{\langle i,j\rangle} \boldsymbol{J}_i \cdot \boldsymbol{J}_j + A\sum_i (\boldsymbol{I}_i \cdot \boldsymbol{J}_i) \tag{S.1}$$

where $V_{ij}^{\mu\nu}$ is the magnetic dipole interaction, $V_{ij}^{\mu\nu} = \frac{\mu_0}{4\pi} \frac{\delta^{\mu\nu}|\vec{r}_{ij}|^2 - 3(\vec{r}_{ij})^\mu (\vec{r}_{ij})^\nu}{|\vec{r}_{ij}|^5}$. $J_{\rm ex}$ is the nearest-neighbor exchange interaction coupling constant. $\mu_B = 0.6717\,\mathrm{K\,T^{-1}}$ is the Bohr magneton, $g_L = \frac{5}{4}$ is a Landé g-factor, and μ_0 denotes vacuum permeability. $\boldsymbol{J}_i$ are angular momentum operators of the Ho^{3+} ions. A is the hyperfine interaction strength, and $\boldsymbol{I}_i$ is the nuclear spin operator, where the total Ho nuclear spin is $I = \frac{7}{2}$. The Ho^{3+} ions may be randomly substituted by nonmagnetic Y^{3+} ions to form $LiHo_xY_{1-x}F_4$. The crystal field term $V_C(\boldsymbol{J}_i)$ imposes an Ising easy axis along the c axis of the crystal, with a first excited state at $\sim 10\,\mathrm{K}$ above the ground-state doublet [3].

Following an approach analogous to that of Chakraborty *et al.* [2] we recast the full Hamiltonian (S.1) as an effective transverse-field Ising model Hamiltonian, but keep the neglected ODD terms. Of the diagonal dipolar terms, we keep only the zz interactions which have been established as the most dominant, but we also keep the off-diagonal interaction terms. The dipolar interaction is invariant under both $i \leftrightarrow j$ and $\mu \leftrightarrow \nu$. We also use the fact that $\left[J_i^x, J_j^z\right] = 0$ and $\left[J_i^y, J_j^z\right] = 0$ when $i \neq j$. In accordance with previous results we also keep only the zz term among the three exchange interaction terms. Additionally, we neglect the hyperfine interaction, as it was found, at least within mean field approximation, not to cause a significant difference in the $B_x - T$ phase diagram in the vicinity of the classical phase transition [4]. The result is the effective Hamiltonian, given in Eq. (1) in the main text, which acts on the full 17-dimensional Hilbert space of the electronic angular momentum. The 2-state Ising space is created anew at each MC operation by determining the two lowest energy states and choosing one of them by the MC rules.

NUMERICAL METHODS

In order to construct approximate many-body states of the full system, we diagonalize the single-site Hamiltonian for each of the sites, given some arbitrary initial set of magnetic moments. Using the magnetic moments obtained for each spin, the fields (2) and ergo single-site Hamiltonians (3) are updated, and the process is repeated until convergence. Convergence is assumed when the absolute difference between the assigned magnetic moment and the magnetic moment dictated by the local field, averaged over all sites, is smaller than $\epsilon_{\rm tol} = 5 \times 10^{-3}\,[\mu_B]$. Within this process, each spin is assumed to be either "up" or "down", as set by the MC simulation, and only the magnitude of its magnetic moment is adjusted. The process is performed following each MC spin-flip. In effect we neglect quantum many-body effects such as entanglement, and instead consider each ion separately. Nevertheless, the single ion is treated exactly by diagonalization of its Hamiltonian in a manner that is self-consistent with all other ions. This method is somewhat similar to the approach described in Ref. [5] under the name inhomogeneous mean-field (iMF), with one important difference. We do not replace the J^z operators in the Hamiltonian with their *thermal* averages but with their quantum mechanical expectation values. Thus we allow the MC simulation to sample thermal fluctuations which are required for the described mechanism to come into effect.

The determination of the single-site energy and magnetic moment is performed as follows: The Hamiltonian (3) is diagonalized numerically and its two low energy levels are designated $|\alpha\rangle$ and $|\beta\rangle$ such that $E_\alpha < E_\beta$. Next, the states $|\alpha\rangle$ and $|\beta\rangle$ are identified as $|\uparrow\rangle$ or $|\downarrow\rangle$ according to their $\langle J^z\rangle$ in the following manner: If $\langle\alpha|J^z|\alpha\rangle > \langle\beta|J^z|\beta\rangle$ then $|\alpha\rangle \equiv |\uparrow\rangle$ and $|\beta\rangle \equiv |\downarrow\rangle$ and vise versa otherwise. Hybridization between the $|\uparrow\rangle$ and $|\downarrow\rangle$ states is suppressed due to the

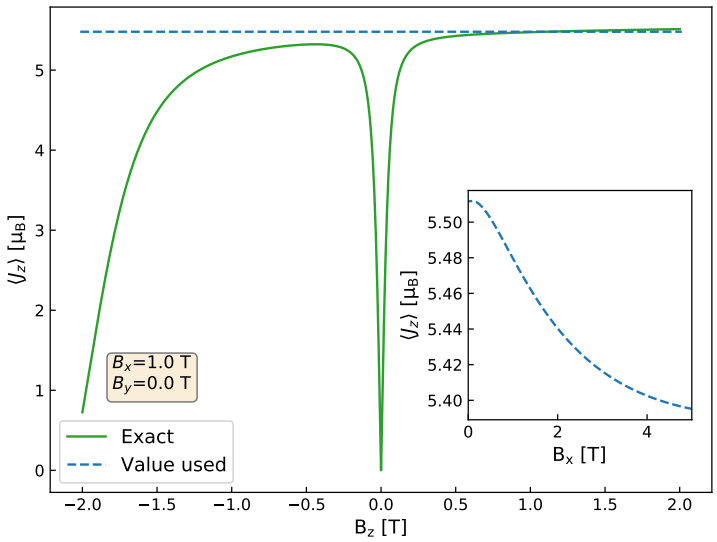

Supplementary Figure 1. The magnetic moment $\langle J^z \rangle$ of the "up" state of a single Ho^{3+} ion as a function of the applied B_z magnetic field, for an applied $B_x = 1\,\mathrm{T}$ field. The solid green line shows the "exact" result (without the hyperfine interaction), which shows significant hybridization when B_z is smaller than $B_x = 1\,\mathrm{T}$. The dashed blue line shows the value used in this work, chosen as described in the text. The inset shows how this value changes as B_x is varied.

hyperfine interaction [6, 7], which we approximately take into account by introducing an artificial longitudinal field in the determination of $\langle J^z \rangle$ that ensures the $|\uparrow\rangle$ and $|\downarrow\rangle$ are not significantly hybridized by the transverse field: For each applied local field, (B_x, B_y, B_z), the B_z component is replaced by $1.1 \times \sqrt{B_x^2 + B_y^2}$ for the purpose of obtaining the magnetic moment. The effect of this process can be seen in Supplementary Figure 1. In practice the energy and magnetic moment are calculated as described on a fixed grid of B_x, B_y and B_z from which they are linearly interpolated during the simulation.

Periodic boundary conditions are used, and the dipolar interaction $V_{ij}^{\mu\nu}$ is calculated using the Ewald summation method without a demagnetization term [8, 9].

We use the parallel tempering Monte Carlo method [10]. To determine the transitions at a given x and B_x we use the finite-size correlation length [8, 11],

$$\xi_L = \frac{1}{2\sin\left(k_{\min/2}\right)} \left[\frac{\left[\langle m^2(0)\rangle_T\right]_{\mathrm{av}}}{\left[\langle m^2(\boldsymbol{k}_{\min})\rangle_T\right]_{\mathrm{av}}} - 1 \right]^{\frac{1}{2}} \tag{S.2}$$

where

$$m(\boldsymbol{k}) = \frac{1}{N} \sum_{i=1}^{N} \langle J_i^z \rangle_\psi \exp(-i\boldsymbol{k} \cdot \boldsymbol{R}_i). \tag{S.3}$$

Here $\langle . \rangle_T$ refers to a thermal average, $[.]_{\mathrm{av}}$ to a disorder average and $\langle . \rangle_\psi$ to a quantum mechanical expectation value. $\boldsymbol{R}_i$ is the location of the site i and $\boldsymbol{k}_{\min} = (\frac{2\pi}{L}, 0, 0)$. The finite-size correlation length divided by the linear system size L has a known scaling form,

$$\frac{\xi_L}{L} \sim \tilde{X}\left(L^{1/\nu}(T - T_c)\right) \tag{S.4}$$

so that for $T = T_c$ it is independent of the system size L. Hence, if a transition exists, curves for different system sizes should cross at the critical temperature. We simulate systems of linear sizes $L = 6, 7, 8$. To find T_c we assume the scaling function (S.4) can be approximated by a third-order polynomial close to the critical point: $f(x) = p_0 + p_1 x + p_2 x^2 + p_3 x^3$ (where $x = L^{1/\nu}(T - T_c)$), and perform a global fit for the six free parameters, $p_0 \ldots p_3$, ν and T_c using the Levenberg-Marquardt algorithm. All 17 individual plots showing the analysis are presented in

Supplementary Figures 2-5. Statistical errors are estimated using the bootstrap method [12]. See Supplementary Tables I-II for numerical results with statistical errors.

Equilibration is verified by logarithmic binning of the data, i.e. the simulation time in terms of MC sweeps is successively increased by a factor of 2, and observables are averaged over that time. When all observables of interest in three consecutive bins agree within error bars, the simulation is deemed equilibrated [12].

For each value of x or B_x the simulation is performed twice: Once with the off-diagonal dipolar terms included in the Hamiltonian (1) and once with these terms omitted so that internal transverse fields are artificially suppressed, i.e. $B_i^x = B_x$ and $B_i^y = 0$ for all i in (2). The self-consistent calculation for the magnetic moments is performed in both cases, as a means to establish its validity.

SIMULATION PARAMETERS

Supplementary tables I-II present the parameters and the results of the Monte Carlo simulations performed for this work.

Supplementary Table I. Simulation parameters at $x = 1$ for different transverse fields B_x and system sizes L, with ODD terms included and excluded. The equilibration/measurement times are 2^b Monte Carlo sweeps. $T_{\min}$ [$T_{\max}$] is the lowest [highest] temperature used and N_T is the number of temperatures. N_{sa} is the number of independent runs. All simulations use $J_{\rm ex} = 1.16\,$mK.

ODD terms	B_x [T]	L	b	$T_{\min}$ [K]	$T_{\max}$ [K]	N_T	N_{sa}	T_c [K]	ν
Included	0.0	6,7,8	10	1.528	1.628	24	50	1.5735(4)	0.65(1)
Excluded	0.0	6,7	10	1.738	1.838	24	50	1.7868(3)	0.59(1)
Excluded	0.0	8	11	1.738	1.838	24	50		
Included	0.3	6,7,8	10	1.512	1.612	24	50	1.5668(4)	0.61(1)
Excluded	0.3	6,7,8	10	1.739	1.839	24	50	1.7800(4)	0.60(1)
Included	0.6	6,7,8	10	1.498	1.598	24	30	1.5529(5)	0.61(1)
Excluded	0.6	6,7,8	10	1.727	1.827	24	30	1.7666(5)	0.60(2)
Included	1.0	6,7,8	10	1.47	1.57	24	30	1.5226(5)	0.64(2)
Excluded	1.0	6,7,8	10	1.705	1.804	24	30	1.7502(5)	0.61(2)
Included	1.5	6,7	10	1.42	1.52	24	30	1.4713(4)	0.56(1)
Included	1.5	8	11	1.42	1.52	24	30		
Excluded	1.5	6,7	10	1.67	1.77	24	30	1.7275(5)	0.62(2)
Excluded	1.5	8	11	1.67	1.77	24	30		

Supplementary Table II. Simulation parameters at $B_x = 0$ for different dilutions $x \leq 1$ and system sizes L, with ODD terms included and excluded. The equilibration/measurement times are 2^b Monte Carlo sweeps. $T_{\min}$ [$T_{\max}$] is the lowest [highest] temperature used and N_T is the number of temperatures. N_{sa} is the number of independent runs.

x	ODD terms	$J_{\rm ex}$ [mK]	L	b	$T_{\min}$ [K]	$T_{\max}$ [K]	N_T	N_{sa}	T_c [K]	ν
1.0	Included	1.16	6,7,8	10	1.528	1.628	24	50	1.5735(4)	0.65(1)
0.83	Included	1.16	6,7,8	10	1.04	1.54	24	200	1.302(2)	0.67(4)
0.67	Included	1.16	6,7,8	10	0.78	1.28	24	350	1.044(2)	0.66(4)
0.46	Included	1.16	6	11	0.39	0.89	24	1000	0.656(2)	0.70(3)
0.46	Included	1.16	7,8	12	0.39	0.89	24	1000		
1.0	Excluded	3.91	6,7,8	10	1.463	1.563	24	30	1.5177(5)	0.59(1)
0.83	Excluded	3.91	6,7,8	10	0.991	1.491	24	200	1.241(2)	0.68(4)
0.67	Excluded	3.91	6,7	10	0.724	1.224	24	350	0.978(2)	0.64(4)
0.67	Excluded	3.91	8	11	0.724	1.224	24	350		
0.46	Excluded	3.91	6	11	0.354	0.854	24	1000		
0.46	Excluded	3.91	7	12	0.354	0.854	24	1000	0.594(2)	0.65(2)
0.46	Excluded	3.91	8	13	0.354	0.854	24	1000		

FINITE-SIZE SCALING ANALYSIS

This section presents the results of the finite size scaling analysis used to obtain T_c from each simulation. For each simulation, the value of B_x and x is set, and then a range of temperatures around T_c is simulated for several system sizes. These simulations are used to obtain the averages required to calculate the finite-size correlation length ξ_L which is used in the finite-size scaling method to obtain an exact estimate of T_c. Supplementary Figures 2-5 show the finite-size scaling results. Despite expected corrections to scaling arising from the relatively small system sizes, all figures show reasonable collapse to a universal curve.

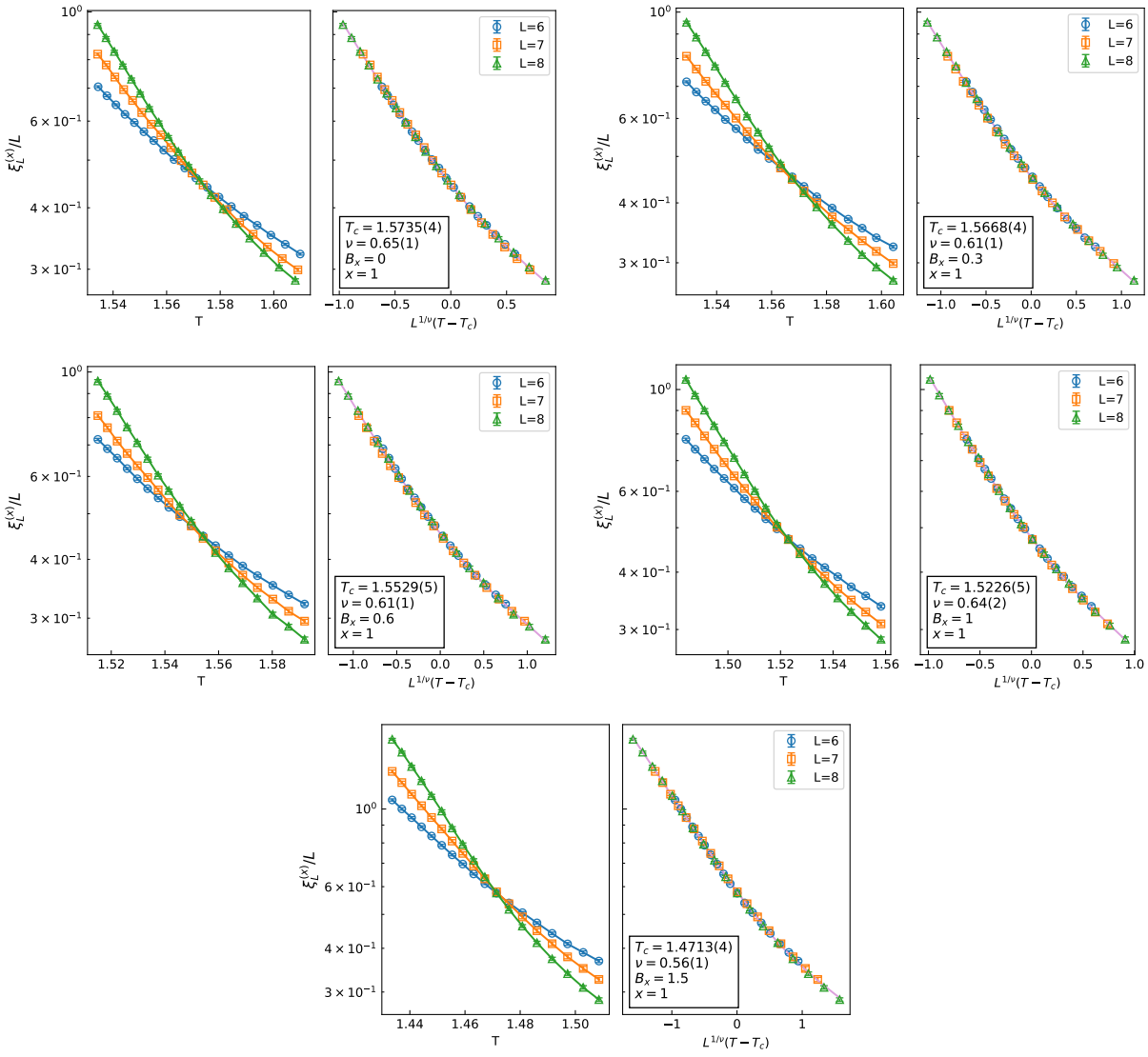

Supplementary Figure 2. Finite size scaling results for simulations with ODD terms included at $x = 1$ and $J_{\text{ex}} = 1.16\,\text{mK}$. Each graph is divided in two: the left side shows the raw results with the curves for different system sizes crossing at T_c and the right side shows the same results with the T axis rescaled showing a collapse onto a universal curve. The parameters for each simulation are listed within the figures.

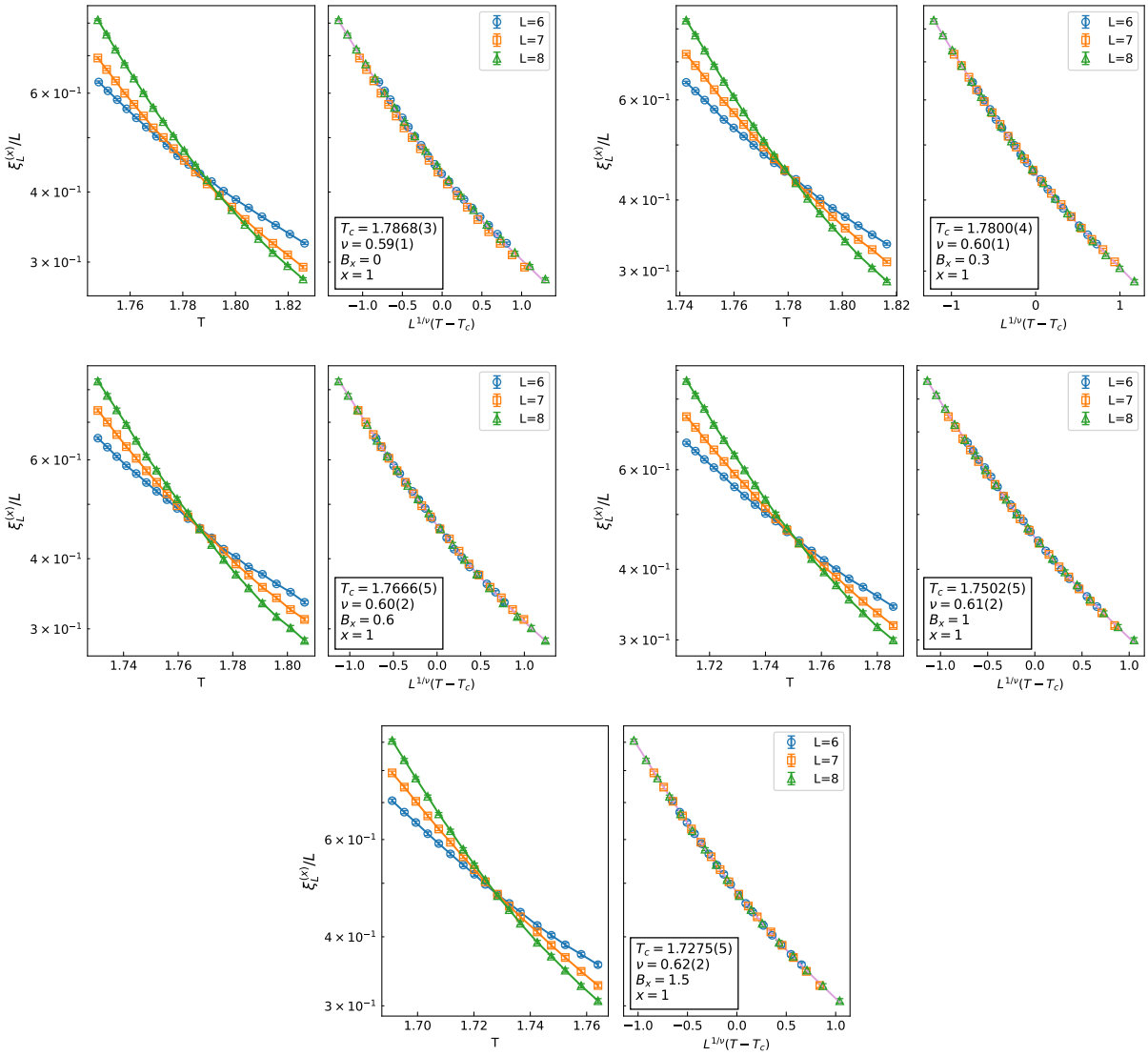

Supplementary Figure 3. Finite size scaling results for simulations with ODD terms excluded. Each graph is divided in two: the left side shows the raw results with the curves for different system sizes crossing at T_c and the right side shows the same results with the T axis rescaled showing a collapse onto a universal curve. The parameters for each simulation are listed within the figures.

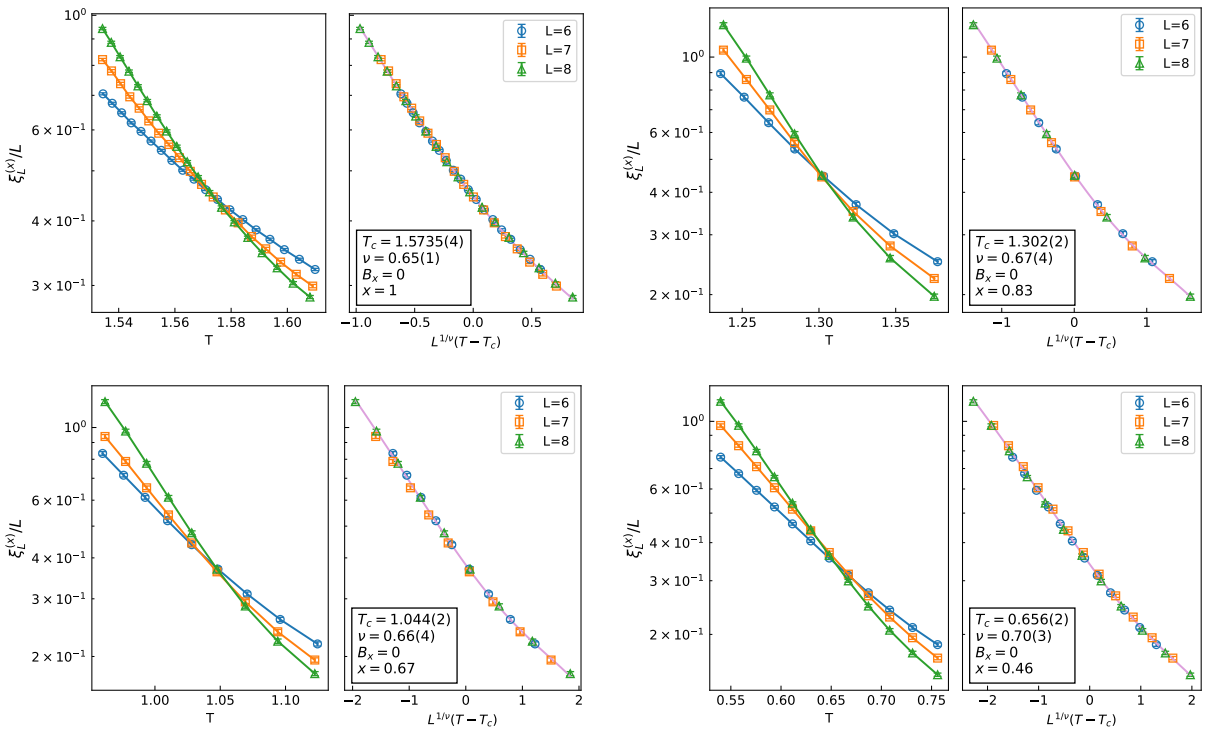

Supplementary Figure 4. Finite size scaling results for simulations with ODD terms included at $x \leq 1$ and $J_{\text{ex}} = 1.16\,\text{mK}$. Each graph is divided in two: the left side shows the raw results with the curves for different system sizes crossing at T_c and the right side shows the same results with the T axis rescaled showing a collapse onto a universal curve. The parameters for each simulation are listed within the figures.

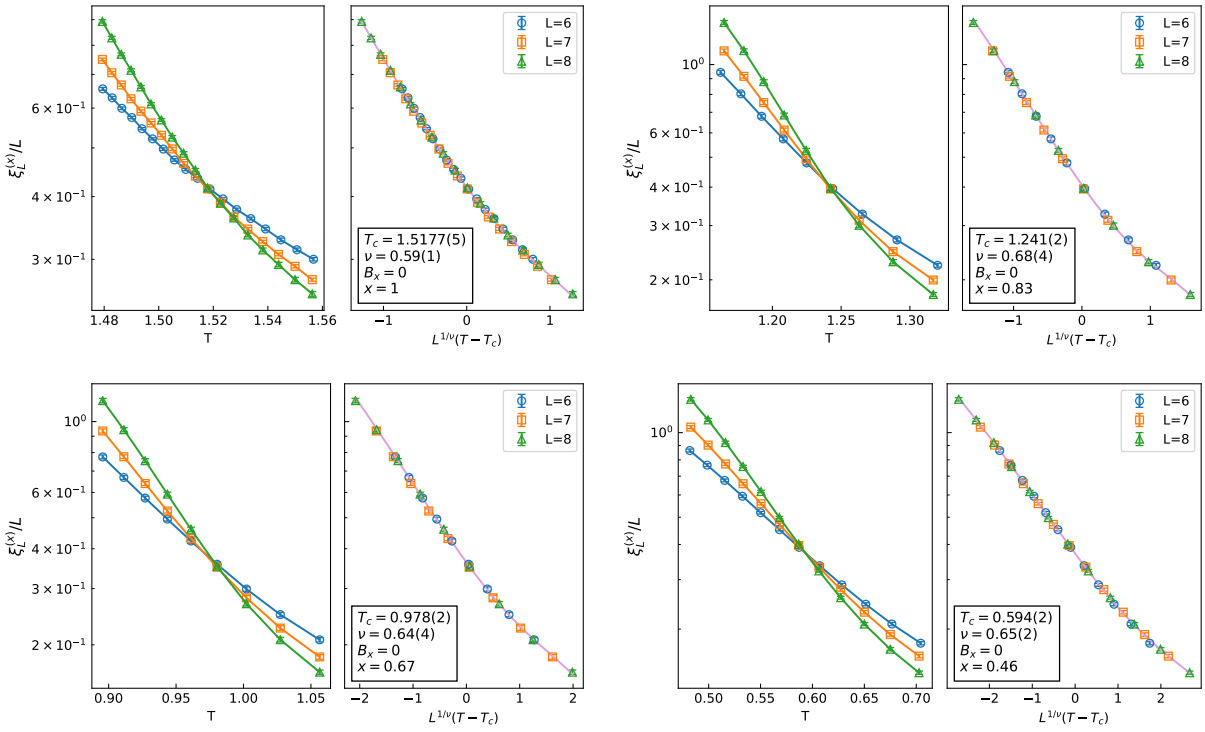

Supplementary Figure 5. Finite size scaling results for simulations with ODD terms excluded at $x \leq 1$ and $J_{\rm ex} = 3.91\,$mK. Each graph is divided in two: the left side shows the raw results with the curves for different system sizes crossing at T_c and the right side shows the same results with the T axis rescaled showing a collapse onto a universal curve. The parameters for each simulation are listed within the figures.

ESTIMATION OF THE EFFECTIVE INTERACTION

The excess change in the energy of the system resulting from the offdiagonal dipolar (ODD) interactions can be viewed, to some extent, as a change in the effective longitudinal (zz) pair interactions. This effective change in the pair interactions is specific to each pair, is dependent on the specific spatial configuration at finite concentration, on transverse magnetic field, and to some extent on the specific configuration of all spins in the system. Yet, it is useful to calculate it in some specific configurations to allow estimation of the contribution of the offdiagonal terms to the energy of the system, and thus to T_c. To calculate the effective interaction due to the ODD mechanism, we take as one example a ferromagnetic system of all spins, except two, in the *up* state. We then calculate the energy of the *full* system for four different configurations of these 2 spins, $E(\uparrow\uparrow)$, $E(\uparrow\downarrow)$, $E(\downarrow\uparrow)$, $E(\downarrow\downarrow)$, where the energy is calculated using $H_{\rm eff}$ given in eq. (1) in the main text, with magnetic moments calculated self consistently as described in the text. The interaction between the two spins is then given by

$$J = \frac{1}{4}\left[E(\uparrow\uparrow) + E(\downarrow\downarrow) - E(\uparrow\downarrow) - E(\downarrow\uparrow)\right]$$

which is a result of the direct longitudinal dipolar interaction, the (nearest-neighbor) exchange interaction and the effective excess interaction due to the ODD mechanism. By repeating the above calculation with and without offdiagonal dipolar terms and subtracting one from the other, we get an estimate of the excess interaction due to the ODD mechanism $J_{\rm eff} \equiv J(\text{ODD included}) - J(\text{ODD excluded})$.

This effective interaction is calculated for pairs of spins along the x axis, along the z axis and for nearest neighbors (which can be seen in Fig. 2a in the main text). Results are obtained for a system of linear size $L = 14$, where dipolar interactions are calculated using the Ewald method. For nearest neighbors the effective interaction is $J_{\rm eff} = -31$ mK (ferromagnetic), for the two closest spins along the x axis it is $J_{\rm eff} = 14$ mK (antiferromagnetic), and for the two closest spins along the z axis it is $J_{\rm eff} = 11$ mK (antiferromagnetic). These values amount to roughly 7-23% of the standard longitudinal dipolar interactions of the respective pairs. Similar results are obtained for an average over a random distribution of the spins.

[1] M. J. P. Gingras and P. Henelius, Collective phenomena in the $LiHo_xY_{1-x}F_4$ quantum Ising magnet: Recent progress and open questions, Journal of Physics: Conference Series **320**, 012001 (2011).

[2] P. B. Chakraborty, P. Henelius, H. Kjønsberg, A. W. Sandvik, and S. M. Girvin, Theory of the magnetic phase diagram of $LiHoF_4$, Phys. Rev. B **70**, 144411 (2004).

[3] H. M. Rønnow, J. Jensen, R. Parthasarathy, G. Aeppli, T. F. Rosenbaum, D. F. McMorrow, and C. Kraemer, Magnetic excitations near the quantum phase transition in the Ising ferromagnet $LiHoF_4$, Phys. Rev. B **75**, 054426 (2007).

[4] D. Bitko, T. F. Rosenbaum, and G. Aeppli, Quantum critical behavior for a model magnet, Phys. Rev. Lett. **77**, 940 (1996).

[5] J. O. Piatek, I. Kovacevic, P. Babkevich, B. Dalla Piazza, S. Neithardt, J. Gavilano, K. W. Krämer, and H. M. Rønnow, Nonequilibrium hysteresis and spin relaxation in the mixed-anisotropy dipolar-coupled spin-glass $LiHo_{0.5}Er_{0.5}F_4$, Phys. Rev. B **90**, 174427 (2014).

[6] M. Schechter and P. C. E. Stamp, Significance of the hyperfine interactions in the phase diagram of $LiHo_xY_{1-x}F_4$, Phys. Rev. Lett. **95**, 267208 (2005).

[7] M. Schechter and P. C. E. Stamp, Derivation of the low-T phase diagram of $LiHo_xY_{1-x}F_4$: A dipolar quantum Ising magnet, Phys. Rev. B **78**, 054438 (2008).

[8] K.-M. Tam and M. J. P. Gingras, Spin-glass transition at nonzero temperature in a disordered dipolar Ising system: The case of $LiHo_xY_{1-x}F_4$, Phys. Rev. Lett. **103**, 087202 (2009).

[9] Z. Wang and C. Holm, Estimate of the cutoff errors in the Ewald summation for dipolar systems, The Journal of Chemical Physics **115**, 6351 (2001).

[10] K. Hukushima and K. Nemoto, Exchange Monte Carlo method and application to spin glass simulations, Journal of the Physical Society of Japan **65**, 1604 (1996).

[11] H. G. Ballesteros, A. Cruz, L. A. Fernández, V. Martín-Mayor, J. Pech, J. J. Ruiz-Lorenzo, A. Tarancón, P. Téllez, C. L. Ullod, and C. Ungil, Critical behavior of the three-dimensional Ising spin glass, Phys. Rev. B **62**, 14237 (2000).

[12] H. G. Katzgraber, M. Körner, and A. P. Young, Universality in three-dimensional Ising spin glasses: A Monte Carlo study, Phys. Rev. B **73**, 224432 (2006).